2011 50th IEEE Conference on Decision and Control and
European Control Conference (CDC-ECC)
Orlando, FL, USA, December 12-15, 2011

Statistical Parameter Estimation and Uncertainty Quantification for Macro Fiber Composite Actuators Operating in Nonlinear and Hysteretic Regimes

Zhengzheng Hu, Ralph C. Smith, Michael Hays and William S. Oates

Abstract— **Macro Fiber Composites (MFC) are planar actuators comprised of PZT fibers embedded in an epoxy matrix that is sandwiched between electrodes. Due to their construction, they exhibit significant durability and flexibility in addition to being lightweight and providing broadband inputs. They are presently being considered for a range of applications including positioning and control of membrane mirrors and configurable aerospace structures. However, due to the noncentrosymmetric nature of PZT, MFC also exhibit hysteresis and constitutive nonlinearities that must be incorporated in models and control designs to achieve their full potential. In this paper, we discuss issues associated with the estimation of parameters and uncertainty quantification (UQ) for a distributed model that quantifies the hysteretic dynamics of the devices. Statistical parameter estimation techniques are used to construct densities for model parameters. These uncertainties are subsequently propagated though the model to construct error bounds.**

I. INTRODUCTION

Macro Fiber Composites (MFC), developed at NASA Langley Research Center, exhibit the capability to generate strains and displacements greater than those that could be obtained by many prior actuators. MFCs consist of active unidirectional piezoceramic fibers embedded in an adhesive polymer matrix with an interdigitated electrode pattern on polyimide films at top and bottom. A detailed overview of the manufacturing process is presented in Williams *et al.* [14]. Due to their flexibility, they can be easily bonded to structures and used to apply or detect strains. The MFC is being considered for a variety of applications including drag, vibration, and noise reduction along with structural health monitoring. It has significant potential for improving the performance of aerospace structures such as rotor blades, jet tailfins and telecommunication satellites.

Since their first fabrication, there has been an increasing number of investigations focusing on the behavior of the MFC. In [16], Williams *et al.* present the response of the MFC to increasing voltage, and provide a model for a piezoelectric continuum subjected to an increase in electric field under constant mechanical load. The same authors discuss in [15] the modeling of the coefficients of thermal expansion for the MFC actuator as a function of temperature. Nonlinearities in the tensile and shear behavior are investigated by Williams *et al.* [17]. In that work, the nonlinear tensile and shear stress-strain behavior and Poisson effects using various plastic deformation models are characterized.

In this paper, we investigate the response of a cantilever beam driven by a MFC actuator patch. The homogenized energy model (HEM) [12], [13] is used to quantify the nonlinear relationship between the electric field applied to the patch and the resulting polarization. It is a multiscale approach in which mesoscopic behavior is quantified by energy principles and a macroscopic model is subsequently constructed using stochastic homogenization techniques. The model was chosen due to its capability for characterizing a range of minor loop behavior under highly varied operating conditions. An Euler-Bernoulli beam model is used to characterize the behavior of the cantilever. Optimization routines are employed to estimate model parameters along with probability density functions (pdf's) charactering their uncertainties. These uncertainties are subsequently propagated though the model to construct error bounds. The displacement of the beam, as a response to different input voltages at the patch, is computed by the model, and used to predict experimental behavior of other input voltages.

In Section II, the experimental setup is summerized. A short description of the homogenized energy model (HEM) and its use to construct a discretized PDE model for a vibrating beam is provided in Sections III and IV. In Section V-A the beam model with polarization quantified by the homogenized energy model is compared with the experimental data. It is illustrated that the model accurately quantifies the nonlinear behavior of the MFC patch in phase space as well as time domain. The uncertainties of the estimated parameters are then analyzed by a bootstrap method in Section V-B. In Section V-C, uncertainties of the model are quantified by constructing error bounds for the displacement of the beam.

II. EXPERIMENTAL SETUP

For the experiments, an aluminum cantilever (with density 2700 $\mathrm{kg/m^3}$, and Young's modulus 69 GPa) was compressed between two aluminum blocks to provide a clamped boundary condition. The cantilever was 114 mm long, 25.4 mm wide and 1 mm thick. At the top side of the cantilever, a MFC actuator of type M-4010-P1 [11] with lateral, expanding

Z. Hu is with the Department of Mathematics, North Carolina State University, Raleigh, NC 27695, USA, zhu4@ncsu.edu

R. C. Smith is with the Department of Mathematics and Center for Research in Scientific Computation, North Carolina State University, Raleigh, NC 27695, USA, rsmith@ncsu.edu

M. Hays is with the Department of Mechanical Engineering, Florida State University, Tallahassee, FL 32306, USA, mrh04c@fsu.edu

W. S. Oates is with the Department of Mechanical Engineering, Florida State University, Tallahassee, FL 32306, USA, woates@eng.fsu.edu

978-1-61284-799-3/11/$26.00 ©2011 IEEE

motion was attached. The driving patch had a thickness of 0.3 mm and the same width as the cantilever and covered the region from 12.7 mm to 55.88 mm measured from the fixed end. The location of the patch was chosen to yield large displacements. In four experiments, an input voltage in the range of 0-100 VDC, 0-200 VDC, 0-400 VDC and 0-800 VDC was applied on the MFC patch. The driving frequency was 1 Hz and the input voltage $V(t)$ (in volts) could be represented by the functions,

$$\begin{aligned} V_i(t) &= 2^{(i-1)} \times 50(1+\sin(2\pi(t-t_i))), \quad i=1,2,4 \\ V_3(t) &= 200+200\cos(2\pi(t-t_3)), \end{aligned} \tag{1}$$

where time t is measured in second and ranges from 0 to 5 seconds in all experiments. In Fig. $1(a)$, all four experimental inputs are plotted as a function of time. As the applied input voltages increase, the patch starts to stretch on top of the cantilever which induces a bending stain in the composite structure and causes out-of-plane deflections. A non-contact capacitor probe was placed 69.85 mm from the fixed end to measure the displacement of the cantilever. Since the device used in the experiments to measure displacement of the beam has no set zero position, all data was shifted so that the displacement is 0 when the input is 0, and all displacements are negative. In Fig. $1(b)$, the resulting displacement data (shifted) is plotted versus the input field $E(t)$ (in MV/m) which is equal to the input voltage divided by the thickness of the patch.

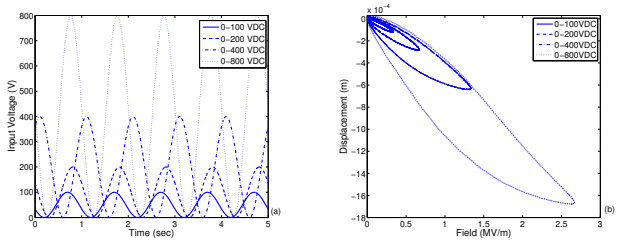

(a) (b)

Fig. 1. (a) Experimental input voltages as a function of time, and (b) measured displacements as a function of input field.

III. Homogenized Macroscopic Polarization Model

To model the polarization response of the MFC to the input voltage, we employed the homogenized energy model (HEM) [12], [13]. In this model, stochastic homogenization techniques are used to incorporate material nonhomogeneities, polycrystallinity, and variable interaction field effects by positing that certain parameters are manifestations of underlying distributions rather than constants. More specifically, the bulk polarization $P(E)$ is formulated as

$$\begin{aligned} [P(E)](t) = \int_0^\infty \int_{-\infty}^\infty \nu_c(E_c)\nu_I(E_I) \\ \times[\bar{P}(E+E_I;E_c,\xi)](t)\,dE_I\,dE_c \end{aligned} \tag{2}$$

where $\bar{P}$ is the local polarization kernel, E is the input electric field, E_I is the field due to dipole interactions, E_c is the coercive field value at which the dipoles switch orientation, and ξ denotes the initial distribution of dipoles. The model parameters E_c and E_I vary through the material and have associated densities ν_c and ν_I.

In this work, the coercive field density function is modeled by a lognormal distribution

$$\nu_c(E_c) = \frac{1}{\sigma_c\sqrt{2\pi}E_c} e^{-\left(\frac{\ln E_c - \ln \bar{E}_c}{\sqrt{2}\sigma_c}\right)^2} \tag{3}$$

whose corresponding normal distribution has mean $\ln \bar{E}_c$, and standard deviation σ_c. The interaction field density function is modeled by a normal distribution

$$\nu_I(E_I) = \frac{1}{\sigma_I\sqrt{2\pi}} e^{-\frac{E_I^2}{2\sigma_I^2}} \tag{4}$$

with mean 0 and standard deviation σ_I.

For general operating regimes, which include the possibility of thermal relaxation mechanisms, it is necessary to include the effects of thermal activation when quantifying $\bar{P}$, and this is accomplished through the Bolzmann relation

$$\mu(G) = Ce^{-GV/kT} \tag{5}$$

which balance the Gibbs energy G and relative thermal energy kT/V. The local polarization is given by

$$\bar{P} = 2P_R x_+ + \frac{E+E_I}{\eta} - P_R \tag{6}$$

where P_R is the remanence polarization, η is the local inverse susceptibility $\dfrac{dE}{dP}$ after switching, and x_+ is the positively oriented dipoles. Here x_+ evolves via the differential equation

$$\dot{x}_+ = -(p_{+-}+p_{-+})x_+ + p_{-+}, \tag{7}$$

involving the likelihoods of switching from negative to positive (p_{+-}) and conversely (p_{-+}). As detailed in [2], we employed the likelihood relations

$$\begin{aligned} p_{+-} &= \frac{1}{\tau}\sqrt{\frac{2V\eta}{\pi kT}}\frac{1}{\operatorname{erfcx}(E_+)}, \\ p_{-+} &= \frac{1}{\tau}\sqrt{\frac{2V\eta}{\pi kT}}\frac{1}{\operatorname{erfcx}(E_-)}, \end{aligned} \tag{8}$$

where $\operatorname{erfcx}(x) = e^{x^2}\dfrac{2}{\sqrt{\pi}}\displaystyle\int_x^\infty e^{-t^2}\,dt$ (the scaled complementary error function), $E_+ = -\sqrt{\dfrac{V}{2kT\eta}}\,(E_c+(E+E_I))$, $E_- = -\sqrt{\dfrac{V}{2kT\eta}}\,(E_c-(E+E_I))$, and τ is the relaxation time. Note that the relaxation time τ is the reciprocal of the frequency at which dipoles attempt to switch.

Let $\gamma = V/kT$, we need to identify seven parameters $p = \{\eta,\ P_R,\ \bar{E}_c,\ \sigma_c,\ \sigma_I,\ \gamma,\ \tau\}$ to calculate the bulk polarization.

Finally, to approximate the double integrals in (2), we used the midpoint rule with integration points E_{c_i}, E_{I_j} and with

the corresponding step sizes v_i and w_j, to yield

$$[P(E)](t) = \sum_{i=1}^{N_i}\sum_{j=1}^{N_j} \nu_c(E_{c_i})\nu_I(E_{I_j}) \times[\bar{P}(E+E_{I_j};E_{c_i},\xi)](t)v_i w_j. \quad (9)$$

Examples of the two sampled densities are shown in Fig. 2.

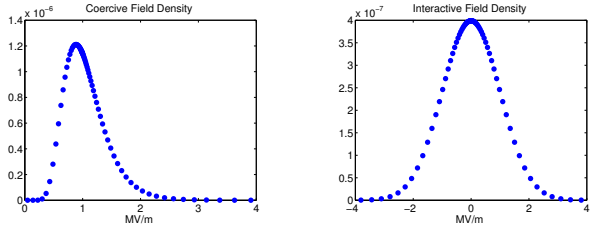

(a) (b)

Fig. 2. (a) Sampled lognormal density ν_c with 80 points. (b) Sampled normal density ν_I with 80 points.

IV. Euler-Bernoulli beam model

To quantify the dynamics of the cantilever in the experiments, we employ an Euler-Bernoulli model. Based on the experimental setup, we consider a thin cantilever beam of length ℓ, width b and thickness h_I that is clamped at $x=0$ and free at $x=\ell$ and a MFC patch with thickness h_A is mounted on the region $[x_1,x_2]$, where $x_1 = 12.7$ mm and $x_2 = 55.88$ mm. We let ρ, α, YI, and cI denote the effective linear density, the air damping coefficient, the stiffness (in terms of the Young's modulus and the geometry) and the combined Kelvin-Voigt damping coefficient, respectively. We also let $w(t,x)$ denote the transverse displacement of the beam at time t. Following the model detailed in Chapter 7 of [12], force and moment balancing yields

$$\rho\frac{\partial^2 w}{\partial t^2} + \alpha\frac{\partial w}{\partial t} - \frac{\partial^2 M}{\partial x^2} = 0 \quad (10)$$

where the moment M is

$$M(t,x) = -YI\frac{\partial^2 w}{\partial x^2} - cI\frac{\partial^3 w}{\partial x^2\partial t} - k[P(E(t))-P(0)]\chi_{pe}(x), \quad (11)$$

and $\chi_{pe}(x)$ is the characteristic function that isolates the input to the region covered by the patch. The polarization P is specified by (2). The system is closed with the boundary and initial conditions

$$w(t,0) = \frac{\partial w}{\partial x}(t,0) = 0, \quad M(t,\ell) = \frac{\partial M}{\partial x}(t,\ell) = 0,$$
$$w(0,x) = \frac{\partial w}{\partial t}(0,x) = 0. \quad (12)$$

In (10), the linear density ρ is given by $\rho(x) = h_I b\rho_I + \chi_{pe}(x)h_A b\rho_A$, with ρ_I and ρ_A being the linear density of the cantilever and the patch, respectively. In (11),

$$YI(x) = Y_I\frac{h_I^3 b}{12} + Y_A c_3\chi_{pe}(x)$$
$$cI(x) = c_I\frac{h_I^3 b}{12} + c_A c_3\chi_{pe}(x)$$

where

$$c_3 = b\int_{h_I/2}^{h_I/2+h_A} z\,dz = \frac{b}{2}\left[\left(\frac{h_I}{2}+h_A\right)^3 - \left(\frac{h_I}{2}\right)^3\right],$$

and Y_I, Y_A, c_I and c_A are the Young's moduli and the Kelvin-Voigt damping coefficients of the cantilever and the patch, respectively.

To solve (10) numerically, we employ the weak formulation

$$\int_0^\ell \rho\frac{\partial^2 w}{\partial t^2}\phi\,dx + \int_0^\ell \alpha\frac{\partial w}{\partial t}\phi\,dx + \int_0^\ell YI\frac{\partial^2 w}{\partial x^2}\frac{\partial^2\phi}{\partial x^2}\,dx + \int_0^\ell cI\frac{\partial^3 w}{\partial x^2\partial t}\frac{\partial^2\phi}{\partial x^2}\,dx = -k[P(E(t))-P(0)]\int_{x_1}^{x_2}\frac{\partial^2\phi}{\partial x^2}\,dx, \quad (13)$$

where $\phi \in H_0^2(0,\ell)$; see Chapter 8 of [12].

More specifically, the modified cubic B-splines $\{\phi_j(x)\}$ subjected to the essential boundary conditions at $x=0$ are used. With N splines (in this work N is taken to be 20), w is approximated by

$$w^N(t,x) = \sum_{j=1}^{N+1} w_j(t)\phi_j(x). \quad (14)$$

For $\mathbf{w} = [w_1(t),\cdots,w_{N+1}(t)]^T$, substitution of (14) into (13), yields the semi-discrete system

$$\mathbb{M}\ddot{\mathbf{w}} + \mathbb{Q}\dot{\mathbf{w}} + \mathbb{K}\mathbf{w} = -k[P(E(t))-P(0)]\mathbf{b} \quad (15)$$

where the mass, damping and stiffness matrices and the force vector are defined by

$$[\mathbb{M}]_{ij} = \int_0^\ell \rho\phi_i\phi_j\,dx \quad (16)$$
$$[\mathbb{Q}]_{ij} = \int_0^\ell \alpha\phi_i\phi_j + cI\phi_i''\phi_j''\,dx \quad (17)$$
$$[\mathbb{K}]_{ij} = \int_0^\ell YI\phi_i''\phi_j''\,dx \quad (18)$$
$$[\mathbf{b}]_i = \int_{x_1}^{x_2}\phi_i''\,dx. \quad (19)$$

To formulate a first-order semi-discrete system that facilitates implementation using standard ODE routines, such as 'ode15s' in MATLAB, we let $\mathbf{z} = [\mathbf{w},\dot{\mathbf{w}}]^T$ and define the system matrix $\mathbb{A}$ and the vector $\mathbf{B}$ by

$$\mathbb{A} = \begin{bmatrix} 0 & \mathbb{I} \\ -\mathbb{M}^{-1}\mathbb{K} & -\mathbb{M}^{-1}\mathbb{Q} \end{bmatrix},$$
$$\mathbf{B} = \begin{bmatrix} 0 \\ -\mathbb{M}^{-1}\mathbf{b} \end{bmatrix}.$$

The second-order system (15) can be subsequently be reformulated as

$$\dot{\mathbf{z}}(t) = \mathbb{A}\mathbf{z}(t) - k[P(E(t))-P(0)]\mathbf{B} \quad (20)$$
$$\mathbf{z}(0) = 0. \quad (21)$$

V. Results

A. Optimization scheme

To identify the seven parameters listed in Sect. III, we consider the minimization problem

$$\hat{p} = \arg\min_{p} \sum_{i=1}^{M} |w^N(t_i, \bar{x}; p) - \hat{w}(t_i)|^2 \qquad (22)$$

where p is the set of parameters, $w^N(t_i, \bar{x}; p)$ is the numerical displacement at $\bar{x} = 69.85$ mm (the observation point in experiments), and $\hat{w}(t_i)$ is the collected experimental data at time t_i. In this work, we have chosen to optimize using the largest input voltage available, 800 VDC. As shown in Fig. 1, displacement data was collected for five identical loading cycles. It is sufficient to use the average displacements of five loading cycles in (23) to estimate parameters. A MATLAB standard nonlinear least-squares optimization scheme, 'lsqnonlin', is evoked for the function defined in (22).

A critical issue when estimating parameters for problems of this type concerns the determination of initial parameters estimates. In [6], we provide data-driven algorithms for estimating parameters in the analogous ferromagnetic homogenized energy model based on major loop magnetization measurements. We are presently investigating the development of robust data-driven algorithms to obtain initial parameter estimates based on minor loop displacement data such as that plotted in Fig. 3. In this investigation, we employed initial estimates based on values obtained in previous investigations for similar devices. The initial parameter values are listed in the second row of Table I and the estimated parameter values are shown in the third row.

The model, with the estimated parameters, is then used to predict the experimental data for the other three input voltages. Figure 3 shows a comparison of the resulting numerical fits (800 VDC), predictions (100, 200, and 400 VDC) and the experimental data. In Fig. $3(a)$, the displacement is plotted versus the electric field, and in Fig. $3(b)$, the displacement is plotted versus time. In Fig. $3(c)$, the simulated polarization is plotted as a function of the electric field. Since the 800 VDC level was used to obtain the model parameters, the fit of the model to that data is the most accurate and the relative error in L_2 norm is 5%. The 200 VDC level shows a good prediction to the data with a 10% relative error. The 100 and 400 VDC levels yield a bigger discrepancy from the data. The relative error of the 100 VDC is 18% and that of the 400 VDC is 19%.

B. Confidence intervals for parameters estimates

In Table I, we summarize the parameter estimates for the seven unknown parameters of the model; however, these values are point estimates only. It is also important to understand the accuracy and reliability of these parameter values. Confidence intervals for the parameters estimates are often used to provide an indication of the reliability of the estimated parameters. More specifically, the wider the derived confidence interval of a parameter, the less reliable the estimated value.

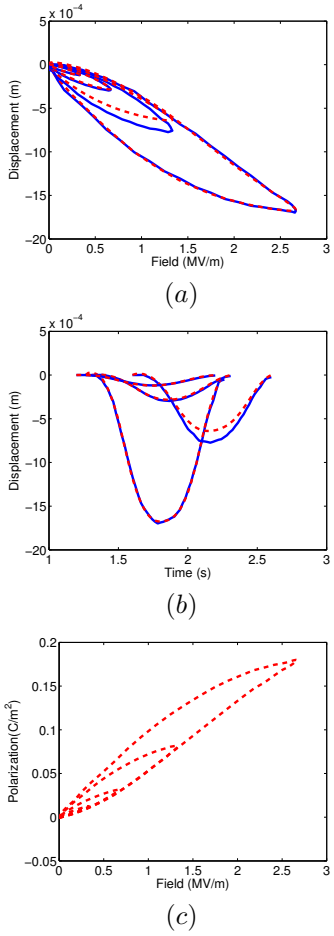

Fig. 3. Model fit to 800 VDC experimental data and model predictions for 100, 200 and 400 VDC data in the (a) phase space and (b) time domain. In (a) and (b), blue solid: experimental data and red dash-lines: simulation results. (c) Modeled polarization plotted versus the electric field.

The traditional asymptotic theory to establish confidence intervals for the estimated parameters involves the calculation of the sensitivity matrix $\chi(\hat{p})$ [1], [3] with components

$$\chi_{ij}(\hat{p}) = \left.\frac{\partial w^N(t_i, \bar{x}; p)}{\partial p_j}\right|_{p=\hat{p}}, \qquad (23)$$

for $i = 1, \cdots, M$, and $j = 1, \cdots, 7$. The covariance matrix V can then be estimated from the relation $V = \sigma^2 \left(\chi^T \chi\right)^{-1}$, where σ^2 is the variance estimate. For this work, the entries of $\chi^T \chi$ (the Fisher Information Matrix) vary from 10^{-10} to 10^7, and based on the singular value decomposition of $\chi^T \chi$, the rank of the matrix is 2. Since the matrix does not have full rank and is poorly conditioned, the matrix inversion can not be carried out with confidence. Therefore, asymptotic theory for this problem does not provide a computationally feasible solution.

As an alternative to the asymptotic theory to derive confidence intervals for the estimated parameters, we employ a wild bootstrap method, which was originally proposed by Wu [18] and rigorously expanded by Liu [7] as a general method for resampling residuals in the presence of error variance heteroscedasticity. The method is referred to as

TABLE I

INITIAL (SECOND ROW) AND IDENTIFIED (THIRD ROW) PARAMETER VALUES OBTAINED THROUGH NONLINEAR LEAST-SQUARES FIT TO THE 800 VDC DATA.

η (m/A)	P_R (C/m^2)	$\bar{E}_c$ (MV/m)	σ_c (dimensionless)	σ_I (MV/m)	γ (m^2/N)	τ (s)
0.8×10^8	0.23	1.0	0.35	1.0	0.6×10^{-2}	0.2×10^{-4}
0.7380×10^8	0.2286	0.8608	0.3485	1.9147	0.6004×10^{-2}	0.2007×10^{-4}

"wild" because n different distributions are estimated from only n observations. The method is summarized below.

First, the least-squares estimate $\hat{p}$ is obtained from (22). Then the residuals $r_i = w(t_i) - w^N(t_i, \bar{x}; \hat{p})$ are calculated for $i = 1, \cdots, M$. The bootstrapped data value $\bar{w}_i^k$ for $k = 1, \cdots, K$ is given by

$$\bar{w}_i^k = w^N(t_i, \bar{x}; \hat{p}) + r_i v_i^k, \tag{24}$$

where each v_i^k satisfies a two-point distribution

$$v_i^k = \begin{cases} \dfrac{1-\sqrt{5}}{2} & \text{with probability } q = (\sqrt{5}+1)/2\sqrt{5} \\ \dfrac{1+\sqrt{5}}{2} & \text{with probability } 1-q. \end{cases}$$

The reader is referred to [4], [8], [9], [10] for more details regarding the definition of the bootstrapped data value $\bar{w}_i^k$.

Finally, the least-squares estimate $\hat{p}^k$ is determined from

$$\hat{p}^k = \arg\min_p \sum_{i=1}^{M} |w^N(t_i, \bar{x}; p) - \bar{w}_i^k|^2. \tag{25}$$

Note that from the bootstrap simulations (25), there are total of K estimates of p. Fig. 4 illustrate the resultant histograms of parameter estimates from the wild bootstrap with $K = 500$. The vertical lines in each plot indicate the original estimates $\hat{p}$. The percentiles of these histograms may be used to construct confidence intervals for $\hat{p}$ [5]. Table II summarizes the 98% confidence intervals for each parameter. From the width of each confidence interval, we observe that P_R, σ_c, γ and τ are most reliable, $\bar{E}_c$ is in the second tier, and σ_I and η are relatively less reliable.

C. Model Uncertainty quantification

The results of the bootstrap method can also be used to approximate the correlation coefficients using the relation

$$\rho_{X,Y} = \frac{\text{cov}(X,Y)}{\sigma_X \sigma_Y} = \frac{\sum_{k=1}^{K}(X-\mu_X)(Y-\mu_Y)}{K\sigma_X\sigma_Y}, \tag{26}$$

where X and Y are bootstrapped results, $\mu_{X,Y}$ is the mean of all K bootstrapped parameter estimates, and $\sigma_{X,Y}$ is the standard deviation of X and Y. The correlation coefficients for all seven parameters are presented in the matrix format

$$\begin{bmatrix} & \eta & P_R & \bar{E}_c & \sigma_c & \sigma_I & \gamma & \tau \\ \eta & 1 & 0.25 & 0.49 & -0.1 & -0.27 & -0.66 & -0.11 \\ P_R & 0.25 & 1 & 0.39 & -0.30 & 0.05 & -0.27 & -0.20 \\ \bar{E}_c & 0.49 & 0.39 & 1 & -0.26 & -0.80 & 0.06 & -0.05 \\ \sigma_c & -0.1 & -0.30 & -0.26 & 1 & 0.01 & -0.22 & -0.17 \\ \sigma_I & -0.27 & 0.05 & -0.80 & 0.01 & 1 & -0.20 & -0.03 \\ \gamma & -0.66 & -0.27 & 0.06 & -0.22 & -0.20 & 1 & -0.28 \\ \tau & -0.11 & -0.20 & -0.05 & -0.17 & -0.03 & -0.28 & 1 \end{bmatrix}.$$

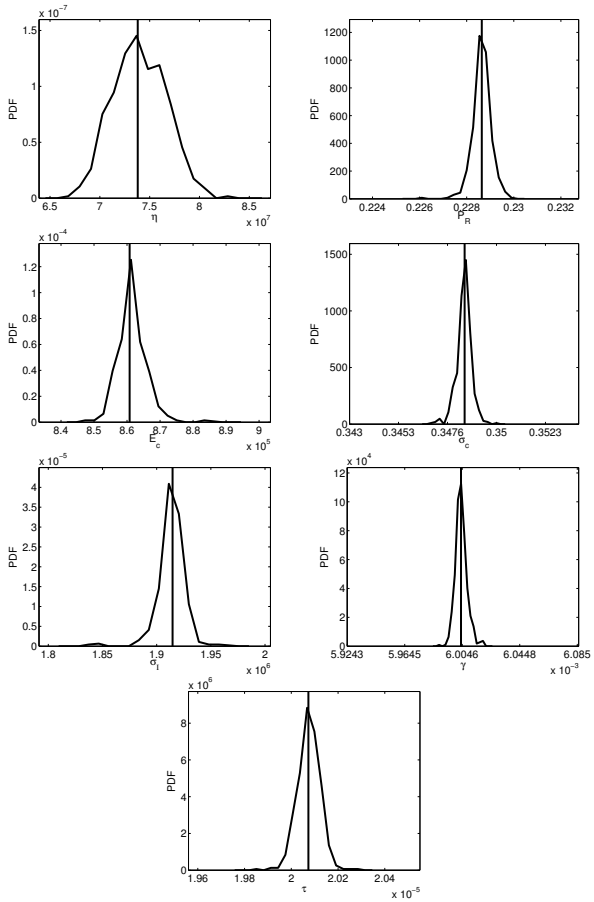

Fig. 4. Histograms of bootstrapped parameter estimates for η, P_R, $\bar{E}_c$, σ_c, σ_I, γ and τ.

We note from the the correlation matrix that the parameter τ is only slightly correlated to all other parameters, with the strongest correlation to γ (note that τ and γ are the two dynamic parameters). However η and $\bar{E}_c$ are strongly correlated to other parameters. This suggests that we perform an uncertainty quantification analysis on τ and $\bar{E}_c$. Here 100 points are sampled from each of the bootstrap results of τ and $\bar{E}_c$, and then combined with nonlinear least-squares estimates (Table I) for the other 5 parameters to form 10,000 parameter sets. The displacements at the observation point are calculated using the Euler-Bernoulli beam model (20)-(21) for the 10,000 parameter sets over a single loading cycle. In Fig. 5, the resultant displacements are plotted together with the corresponding error bars (two standard deviations).

TABLE II

98% CONFIDENCE INTERVALS DERIVED FROM THE WILD BOOTSTRAP METHOD USING THE PERCENTILE METHOD.

$\eta/10^8$ (m/A)	P_R (C/m^2)	$\bar{E}_c$ (MV/m)	σ_c (dimensionless)	σ_I (MV/m)	$\gamma/10^{-2}$ (m^2/N)	$\tau/10^{-4}$ (s)
(0.6826, 0.8019)	(0.2275, 0.2296)	(0.8518, 0.8731)	(0.3472, 0.3493)	(1.8491, 1.9390)	(0.5995, 0.6017)	(0.1995, 0.2019)

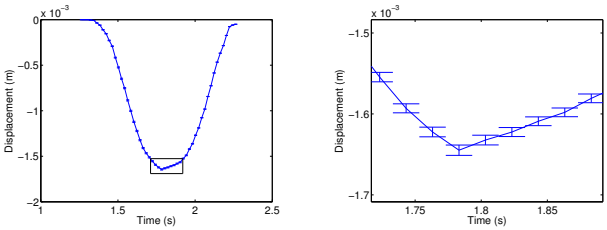

(a) (b)

Fig. 5. (a) Displacement results for the 10,000 parameter sets with error bars showing two standard deviations. (b) Expansion of the region around the maximum displacement.

We observe that all error bars are very small with the largest values coincide with the maximum of the displacements.

VI. CONCLUSIONS

The results of the numerical simulations show that the beam model in combination with the homogenized energy model is able to accurately describe the nonlinear behavior of a structure driven by a MFC patch. The estimated parameters for the 800 VDC driving regime yield a model that accurately predicts at the other drive levels. The uncertainty analysis of the estimated parameters, using a "wild" bootstrap method, yields non-Gaussian behavior for some of parameters; e.g., $\bar{E}_c$, P_R and σ_I. The confidence intervals of each parameter suggest that the estimated values of P_R, σ_c, γ and τ are most reliable. The error bars of displacements using the parameter values from the bootstrap results are very small with the largest errors coinciding with the maximum of displacements. We are currently determining error bounds from the experiments for further analysis.

In the future, we will investigate the formulation of the homogenized energy model for 90° ferroelastic switching in the MFC. Whereas the 180° switching model employed here accurately characterizes the MFC dynamics, it is relying on phenomenological properties of ferroelectric switching. The 90° ferroelastic switching more physically quantifies the material behavior that produces strains and hence displacements in PZT-based devices such as MFC and THUNDER.

VII. ACKNOWLEDGMENTS

This research of ZH was supported through the NSF Grant DMS-0636590, EMSW21-RTG program while the research of RCS was supported in part by the Air Force Office of Scientific Research through the grant AFOSR-FA9550-08-1-0348. The research of MH and WSO was supported by the Florida Center for Advanced Aero Propulsion (FCAAP) and an AFOSR grant FA9550-09-1-0353.

REFERENCES

[1] H. T. Banks, M. Davidian, J. R. Samuels, Jr. and K. L. Sutton, "An inverse problem statistical methodology summary," *Workshop on Biomedical Modeling and Cardiovascular-Respiratory Control*, Schloss Seggau, Leibnitz, Austria, 2007; CRSC Technical Report CRSC-TR08-01.

[2] T. R. Braun and R. C. Smith, "High speed model implementation and inversion techniques for ferroelectric and ferromagnetic transducers," *J. of Intelligent Material Systems and Structures*, 19(11):1295-1310, 2008.

[3] A. Cintron-Arias, H. T. Banks, A. Capaldi and A. L. Lloyd, "A sensitivity matrix based methodology for inverse problem formulation," *J. of Inverse and Ill-Posed Problems*, 17:545-564, 2009.

[4] R. Davidson and E. Flachaire, "The wild bootstrap, tamed at last," *J. of Econometrics*, 146(1):162-169, 2008.

[5] B. Efron and R. J. Tibshirani, *An introduction to the bootstrap*, New York: Chapman & Hall, 1993.

[6] Z. Hu and R. C. Smith, "Data-driven techniques to estimate parameters in a rate-dependent ferromagnetic hysteresis model," Submitted to Physica B, Special Issue: HMM 2011.

[7] R. Y. Liu, "Bootstrap procedures under some non-i.i.d. models," *Annals of Statistics*, 16(4):1696-1708, 1988.

[8] J. G. MacKinnon, "Bootstrap methods in econometrics," *The Economic Record*, 82:S2- S18, 2006.

[9] E. Mammen, "Bootstrap and wild bootstrap for high dimensional linear models," *Annals of Statistics*, 21(1):255-285, 1993.

[10] J. Matthews, "Sensitivity analysis and development of a model that quantifies the effect of soil moisture and plant age on leaf conductance," Ph.D Dissertation, North Carolina State University, Raleigh, NC, 2010.

[11] Smart Materials, http://www.smart-material.com/MFC/P1_types.php

[12] R. C. Smith, *Smart Material Systems - Model Development*, SIAM, Philadelphia, 2005.

[13] R. C. Smith, S. Seelecke, Z. Ounaies and J. Smith, "A free energy model for hysteresis in ferroelectric materials," *J. of Intelligent Material Systems and Structures*, 14(11):719-739, 2003.

[14] R. B. Williams, B. W. Grimsley, D. J. Inman and W. K. Wilkie, "Manufacturing and mechanics-based characterization of macro fiber composite actuators," In *Proceedings of the 2002 ASME International Adaptive Structures and Materials Systems Symposium*, New Orleans, LA, November 17-22, 2002.

[15] R. B. Williams, D. J. Inman and W. K. Wilkie, "Temperature-dependent coefficients of thermal expansion for macro fiber composite actuators," In *Proceedings of the 5th International Congress on Thermal Stresses*, Blacksburg, VA, June 8-11, 2003.

[16] R. B. Williams, D. J. Inman and W. K. Wilkie, "Nonlinear response of the macro fiber composite actuator to monotonically increasing excitation voltage," *J. of Intelligent Material Systems and Structures*, 17:601-608, 2006.

[17] R. B. Williams, M. R. Schultz, M. W. Hyer, D. J. Inman and W. K. Wilkie, "Nonlinear tensile and shear behavior of macro fiber composite actuators," *J. of Composite Materials*, 38(10):855-869, 2004.

[18] C. F. J. Wu, "Jackknife, bootstrap and other resampling methods in regression analysis," *Annals of Statistics*, 14(4):1261-1295, 1986.